Colloids and Surfaces B: Biointerfaces 224 (2023) 113216

Contents lists available at ScienceDirect

Colloids and Surfaces B: Biointerfaces

journal homepage: www.elsevier.com/locate/colsurfb

The interaction of tryptophan enantiomers with model membranes is modulated by polar head type and physical state of phospholipids

Alexa Guglielmelli [a,b], Rosa Bartucci [c,*], Bruno Rizzuti [b,d], Giovanna Palermo [a,b], Rita Guzzi [e,b], Giuseppe Strangi [a,b,f]

[a] Department of Physics, NLHT Lab., University of Calabria, 87036 Rende, Italy
[b] CNR NANOTEC-Institute of Nanotechnology, SS Rende (CS), 87036 Rende, Italy
[c] Department of Chemistry and Chemical Technologies, Molecular Biophysics Laboratory, University of Calabria, 87036 Rende, Italy
[d] Institute for Biocomputation and Physics of Complex Systems (BIFI), Joint Unit GBsC-CSIC-BIFI, University of Zaragoza, 50018 Zaragoza, Spain
[e] Department of Physics, Molecular Biophysics Laboratory, University of Calabria, 87036 Rende, Italy
[f] Department of Physics, Case Western Reserve University, 2076 Adelbert Rd, Cleveland, OH 44106 USA

ARTICLE INFO

Keywords:
Tryptophan stereoisomers
DPPC
DDPG
ATR-FTIR
ESR
Molecular docking

ABSTRACT

The mutual influence of chiral bioactive molecules and supramolecular assemblies is currently being studied in many research fields, including medical-pharmaceutical applications. Model membranes of phospholipids, such as the zwitterionic dipalmitoylphosphatidylcholine (DPPC) and the anionic dipalmitoylphosphatidylglycerol (DPPG), interact with a variety of chiral compounds that include amino acids. In this work, the interaction of tryptophan enantiomers, L-Trp and D-Trp, on DPPC and DPPG bilayers was investigated by using differential scanning calorimetry, attenuated total reflectance-Fourier transform infrared and spin-label electron spin resonance spectroscopies as well as molecular docking simulations. The results show that Trp enantiomers slightly perturb the bilayer thermotropic phase transitions. For both membranes, O atoms in the carbonyl groups have a propensity to act as acceptors of a (weak) hydrogen bond. The Trp chiral forms also promote formation of hydrogen bonds and/or hydration in the PO_2^- moiety of the phosphate group, especially for the DPPC bilayer. In contrast, they interact more closely with the glycerol group of DPPG polar head. Only for DPPC bilayers, both enantiomers increase the packing of the first hydrocarbon chain segments for temperatures through the gel state, whereas they do not affect the lipid chain order and mobility in the fluid state. The results are consistent with a Trp association in the upper region of the bilayers without permeation in the innermost hydrophobic region. The findings suggest that neutral and anionic lipid bilayers are differently sensitive to amino acid chirality.

1. Introduction

Inside the human body many fundamental biomolecules, such as amino acids (AAs), sugars, lipids, and nucleotides are chiral, so that each isomer cannot be superimposed on its mirror image. Chiral molecules and their mirror counterparts are identified as enantiomers, labeled with L- or D- depending on their ability to rotate the plane of polarized light. In principle, apart from their optically active behavior, the two enantiomers are physically and chemically identical molecular species when considered in isolation. Nevertheless, biosystems interact with chiral ligands in very specific ways. For example, an enzyme (or a protein) usually has a binding pocket that matches more favorably, or even exclusively, with only one enantiomer [1]. At the same time, stereospecificity has been reported in the interaction of lipid membranes with chiral compounds [2–8]. It is worthy to note that the bioactivity of the enantiomers of a given compound can be dramatically different, causing dissimilar physiological and pharmaceutical effects, as it famously occurred for the racemic drug thalidomide: while the D- form was safe, its mirror image turned out to be teratogenic [9,10]. Stereoisomers of metabolites and AAs are also differently involved in many biological processes, so that they can be considered for noninvasive clinical diagnosis and biomarkers screening [11–16]. Moreover, the process of AAs chiral inversion in various peptides seems related to the development of many pathologies, including Alzheimer's and Parkinson's disease, and type II diabetes [17].

Among AAs, tryptophan (Trp) holds a prominent role in

* Corresponding author.
E-mail address: rosa.bartucci@fis.unical.it (R. Bartucci).

https://doi.org/10.1016/j.colsurfb.2023.113216
Received 18 November 2022; Received in revised form 29 January 2023; Accepted 21 February 2023
Available online 23 February 2023

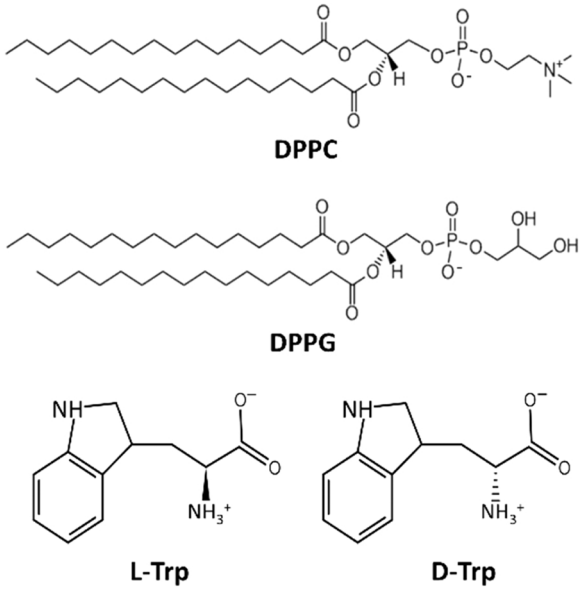

Fig. 1. Chemical structures of the neutral lipid dipalmitoylphosphatidylcholine (DPPC), the anionic lipid dipalmitoylphosphatidylglycerol (DPPG), and tryptophan enantiomers (L- and D-Trp).

physiopathological processes. As precursor of serotonin, melatonin and niacin (B3 vitamin), it participates indirectly to many metabolic and cognitive functions, by affecting sleep, mood, and mental health [18–20]. It is, therefore, of interest to investigate whether L-Trp and the chiral counterpart D-Trp exert specific effects upon interacting with cell membrane components, as well as with supramolecular lipid aggregates. Several literature studies have characterized different aspects of Trp/lipid membrane interactions, showing that this AA affects the structure and dynamics of various model membranes [21–25]. However, studies focusing on Trp chiral specificity are rather sparse. For instance, lipid membranes of a single lipid species have been proposed to represent a platform for chiral recognition of AAs, including Trp [3].

The aim of this work is to explore how the molecular properties of model lipid membranes change upon their interaction with Trp enantiomers. For this purpose, fully hydrated bilayers composed by single species of phospholipids were studied in buffer solution at physiological pH in the absence and in the presence of L- and D-Trp. The lipids we used are the neutral zwitterionic lipid dipalmitoylphosphatidylcholine (DPPC) and the anionic lipid dipalmitoylphosphatidylglycerol (DPPG) (Fig. 1), that are among the most abundant in cell membranes [26]. Both are L-glycerophospholipids containing carbonyl ester C═O groups and bearing the same saturated aliphatic chains of sixteen C atoms, but with different polar heads: that of DPPC has a dipole pointing from the O^- to the N^+ of the choline, whereas the polar head of DPPG has a negatively charged O^- and the glycerol moiety. From a chemical standpoint, Trp (Fig. 1) is an aromatic AA with amphiphilic character for the presence of a hydrophobic indole ring in the side chain. At physiological pH it is zwitterionic, with the α-amino group protonated (NH_3^+; $pK_a = 9.39$) and the α-carboxylic acid group deprotonated (COO^-; $pK_a = 2.38$).

The effects of the binding of the L-Trp and D-Trp enantiomers on the membrane properties were studied on a multiscale level by using differential scanning calorimetry (DSC), attenuated total reflectance-Fourier transform infrared (ATR-FTIR), and spin-label electron spin resonance (ESR) spectroscopy of lipids spin-labeled at two different carbon atom positions, C_n, along the chain (n-PCSL), to probe the first acyl chain segments (4-PCSL), and the terminal methyl ends (14-PCSL) of the bilayers. Experiments were complemented with molecular docking simulation to get insight into the molecular interactions of isolated DPPC and DPPG phospholipids with Trp.

The overall results are consistent with the interaction of the two Trp forms with the polar/apolar interfaces of the membrane. The enantiomeric specificity is weak and the observed effects appear to be modulated by the nature of the lipid polar head (i.e., phosphatidylcholine versus phosphatidylglycerol) and the physical state (i.e., gel versus liquid-crystalline) of the lipid membranes.

2. Materials and methods

2.1. Materials

The synthetic lipids 1,2-dipalmitoyl-*sn*-glycero-3-phosphocholine (DPPC) and 1,2-dipalmitoyl-*sn*-glycero-3-phospho-1′-rac-glycerol (DPPG) were from Avanti Polar Lipids. The spin-labeled phosphatidylcholines (1-palmitoyl-2-stearoyl-(n-doxyl)-*sn*-glycero-3-phosphocholine, n-PCSL, n = 4 and 14) were synthesized as described in [27]. L-Trp, D-Trp and Dulbecco's phosphate-buffered saline (DPBS, 10 mM, pH 7.4) were purchased from Sigma-Aldrich. All materials were used as obtained, without further purification.

2.2. Sample preparation

Samples used in this study are model membranes in the form of multilamellar lipid dispersions, known as liposomes, and hereafter referred to as lipid bilayers, prepared according to the thin film hydration method [28]. DPPC and DPPG films were formed from lipid solutions in chloroform or chloroform/methanol (2:1 v/v), and dried first under a gentle nitrogen gas stream and then under vacuum overnight, to ensure proper solvent removal. The dry lipid films were fully hydrated either in DPBS or in DPBS containing 15 mol% of L-/D-Trp by heating at 50 °C, a value above the lipid bilayers main phase transition temperature, and vortexing until an opalescent bilayer suspension was obtained. Solutions containing Trp were prepared by dilution from a concentrated stock solution (35 mM) in DPBS at pH 7.4. Trp concentration was determined by using a molar extinction coefficient of 5690 M^{-1} cm^{-1} at the optical absorption wavelength maximum, $\lambda_{max} = 278$ nm [29]. For all the experiments, the samples were left to incubate at T = 25 °C for 48 h before performing any measurement. This sample handling procedure, previously used in other similar studies to investigate the adsorption of AAs on lipid bilayers (see, for instance [3]), does not affect the integrity of the bilayers, as reproducible values of the optical density at 400 nm ($OD_{400} \approx 2.0$–2.5) were obtained before and after incubation. The concentration of Trp enantiomers is typically that used to experimentally investigate AAs/membrane interaction, as it produces appreciable changes in the membranes without compromising their structure, and the incubation time was chosen in order to reach an equilibrium in the L-/D-Trp adsorption on lipid membranes [3]. Multilamellar lipid bilayers were preferred over other lipid mesophases, such as large or small unilamellar vesicles, for their stability over time and versatility of experimental use, giving rise to defined and reproducible calorimetric thermotropic phase transitions, EPR spectra and ATR-FTIR bands.

2.3. Differential scanning calorimetry (DSC)

For DSC measurements, DPPC and DPPG bilayers were prepared either pure or with 15 mol% of L-/D-Trp, at the final lipid concentration of 1.36 mM in 1 mL of DPBS at pH 7.4. DSC experiments were performed on a VP-DSC MicroCalorimeter (MicroCal, Inc), having a cell volume of 0.52 mL and a temperature resolution of 0.1 °C. The thermograms were collected on heating at a rate of 5 °C/h within the temperature range 20–50 °C. The data were analyzed by using the Origin software (MicroCal). The excess heat capacity function, C_p, was obtained after solvent baseline subtraction, normalization by the lipid concentration, and linear fitting of the baseline before and after the transitions. Phase transition temperatures, T_p and T_m, were determined as the values corresponding to the maximum heat capacity, whereas enthalpies, ΔH_p and ΔH_m, were obtained by integrating the area under the

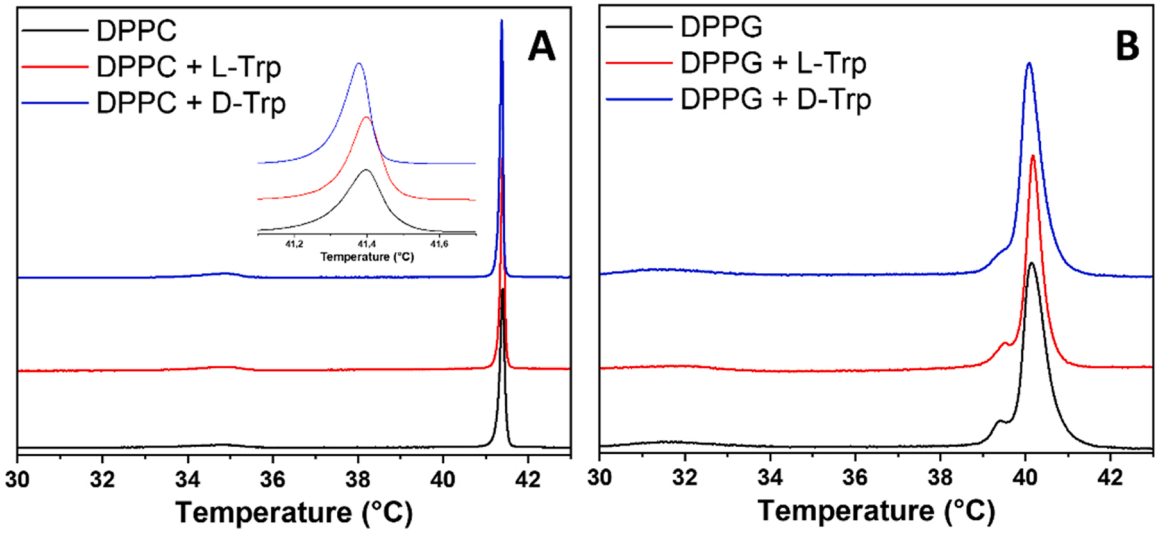

Fig. 2. DSC thermograms for (A) DPPC and (B) DPPG bilayers, without (bottom line, black) and with L-Trp (middle line, red) or D-Trp (top line, blue) enantiomers, hydrated in DPBS at pH 7.4. The curves are vertically shifted and a zoom of the region encompassing the DPPC main phase transition is provided to improve visualization. (For interpretation of the references to color in this figure legend, the reader is referred to the web version of this article.)

corresponding transition peaks in the thermal profile. Main transition width at half height, $\Delta T_{m,1/2}$, were also evaluated to assess the phase transition cooperativity: an increase of $\Delta T_{m,1/2}$ corresponds to a decrease in cooperativity.

2.4. Attenuated total reflectance Fourier-transform infrared (ATR-FTIR) spectroscopy

Temperature-dependent ATR-FTIR measurements on bilayers without and with Trp at the final lipid concentration of 8.2 mM in 0.5 mL of DPBS at pH 7.4 were carried out on a Tensor II spectrometer (Bruker Optics), equipped with a liquid nitrogen cooled mercury cadmium telluride detector and a BioATR II cell with a silicon crystal. The cell was thermostated by a refrigerated circulator bath (Huber Ministat 125 Pilot One). The amount of 20 μL from the samples was incubated for 30 min at the starting temperature before data collection. IR spectra of both the background (solvent) and the lipid suspension were collected on heating in the temperature range 24–48 °C, with a temperature step $\Delta T = 2$ °C and equilibration time of 2 min. After measuring the signal from the background, the cell was cleaned and filled with the lipid sample. For both the solvent and the sample measurements, data from 120 scans were collected and averaged. Spectra were recorded in the 4000–900 cm^{-1} wavenumber range with a 4 cm^{-1} resolution. Post zero-filling (4 points) was applied to improve spectral resolution. For data analysis, raw data of original spectra were processed using the OPUS 7.5 software package. Bandwidths were measured at 75 % of height of the peak maximum from baseline corrected spectra. Peak deconvolutions were carried out as described previously [30] with a Pearson VII function by using the multiple peak fit module in the Origin software.

2.5. Spin-label electron spin resonance (ESR) spectroscopy

ESR experiments were performed on samples prepared as described above at the final lipid concentration of 50 mM in 200 μL DPBS at pH 7.4, and spin-labeled by codissolving the lipids with 1 mol% of the spin-label. Spin-labeled bilayer suspensions were transferred into 100 μL glass capillaries and immediately sealed. ESR spectra were acquired on a Bruker ESP-300 spectrometer operating at 9 GHz with 100-kHz field modulation, and equipped with a temperature controller ER 4111 VT as well as a rectangular cavity ER 4201 TE_{102}, both from Bruker. Sample capillaries were placed in a standard 4 mm quartz sample tube with light silicone oil for thermal stability, and positioned in the center of the cavity. ESR spectra were recorded well below saturation of the signal, at a microwave power of 10 mW with 1–1.5 G_{p-p} magnetic field modulation amplitude, and multiple scans were accumulated to increase the signal-to-noise ratio.

In any type of experiment, two independent measurements on newly prepared samples were executed to test data reproducibility. The data points are reported as mean ± standard error, where the standard error is the semidispersion of the data.

2.6. Molecular docking simulation

Molecular docking was carried out by using the software AutoDock Vina version 1.2.3 [31], which allows one to perform the simultaneous docking of multiple ligands. The structures of both L-Trp and D-Trp enantiomers and of the two phospholipid molecules DPPC and DPPG were taken from PubChem [32]. To reduce the number of degrees of freedom in the molecular system, the last 14 C atoms in the acyl chain of the phospholipid molecules were truncated, because Trp does not bind to such region on the basis of our spectroscopic results and other simulation techniques [33]. Full flexibility was allowed for the AA in either chirality during the docking, as well as for the phospholipid molecules. Two (or three in some initial test cases) molecules of either DPPC or DPPG were docked to either Trp enantiomers in each *in silico* experiment.

In the docking calculations, Trp was considered the host and the phospholipid molecules of either species as guests. The AA was placed at the center of a search volume of size 20 Å × 20 Å × 20 Å, and the search was performed with standard exhaustiveness [34]. This procedure was repeated five times in each case, leading to an ensemble of different docking complexes due to the inherent stochasticity in the search process of AutoDock Vina, which is a Monte-Carlo iterated algorithm combined with a gradient-based optimizer [35]. The eight most favorable docking poses were taken for each simulation run, after excluding the complexes in which the two phospholipids formed a large angle (> 90°) with each other, as their direction is statistically expected to be roughly parallel when their chains are inserted into the common membrane core. The docking poses analyzed after this screening stage differed from each other by 0.2–0.3 kcal/mol, which is within the limit of accuracy expected for the scoring function of AutoDock Vina [31].

Table 1
Temperature and enthalpy for the pre- (T_p and ΔH_p) and main (T_m and ΔH_m) phase transitions of DPPC and DPPG bilayers with and without L-/D-Trp hydrated in DPBS at pH 7.4. The width at half height of the main transition, $\Delta T_{m,1/2}$, is also reported. The error on temperature is ± 0.1 °C and on enthalpy is 2 %.

	T_p (°C)	ΔH_p (kcal/mol)	T_m (°C)	ΔH_m (kcal/mol)	$\Delta T_{m,1/2}$ (°C)
DPPC	34.8	1.3	41.4	8.3	0.12
+ L-Trp	34.9	2.2	41.4	10.3	0.09
+ D-Trp	34.8	1.6	41.4	8.6	0.08
DPPG	31.5	0.7	40.1	8.4	0.59
+ L-Trp	32.0	0.6	40.1	6.5	0.40
+ D-Trp	31.2	0.7	40.1	7.8	0.52

3. Results

3.1. Differential scanning calorimetry

DSC measurements provide information regarding the effect of Trp enantiomers on the phase transitions of DPPC and DPPG bilayers. Fig. 2A and B show, respectively, the DSC heating thermograms of DPPC and DPPG model membranes, both pure and in the presence of either L- or D-Trp.

From the thermal profiles are evident the two endothermic transitions of DPPC and DPPG membranes. The first is the low-temperature and low-energy pre-transition, arising from the conversion of the lamellar gel phase $L_{\beta'}$ to the rippled gel phase $P_{\beta'}$, occurring at T_p; the second one is the high-temperature and high-energy main-transition, corresponding to the conversion to the liquid-crystalline state L_α occurring at T_m. The transition characteristics (i.e., temperatures, T_p or T_m, enthalpies, ΔH_p or ΔH_m, and main transition bandwidth, $\Delta T_{m,1/2}$) (see Table 1) are consistent with literature data on DPPC and DPPG samples investigated under experimental conditions similar to those used in this study [36,37].

For DPPC bilayers, the temperature values of the pre- and the main transition remained unaltered with the addition of L- or D-Trp; in contrast, the enthalpies of both transitions and the cooperativity of the main-transition increased, and, therefore, $\Delta T_{m,1/2}$ decreased, with the presence of the two enantiomers, especially for L-Trp (Fig. 2A and Table 1). This is consistent with cohesive lipid interactions and sharpening of the gel-to-fluid phase transition promoted by Trp addition to DPPC. Previous DSC data reported that L-Trp induced stabilization of the DPPC chain packing by increasing T_m and ΔH_m, whereas D-Trp left almost unperturbed the membrane thermotropic phase behavior [3]. The discrepancy of these reports with our data could be ascribed to the different experimental conditions used (i.e., type of lipid mesophases and acquisition scan rates of the thermograms). For DPPG bilayers, with respect to the pure anionic membrane, T_p is upshifted by 0.5 °C, ΔH_m is decreased of about 2 % and $\Delta T_{1/2}$ of about 0.2 °C in DPPG/L-Trp sample; the phase transition characteristics were less affected in DPPG/D-Trp sample (Fig. 2B and Table 1). Therefore, at variance with what observed for the neutral DPPC, in the anionic DPPG matrix the presence of Trp enantiomers weakens the lipid interactions and makes the main transitions more cooperative, particularly in the case of L-Trp.

The DSC findings indicate that the Trp enantiomers, upon interacting with DPPC and DPPG bilayers, induce dissimilar small perturbations to the thermotropic phase behaviors. Such a kind of small perturbations is typical of external agents that act on the lipid surfaces without penetrating deeply in the hydrocarbon membrane region.

3.2. Attenuated total reflectance – Fourier transform infrared spectroscopy

In order to explore the interaction between DPPC and DPPG membranes with L-/D-Trp at the level of single molecular groups, temperature-dependent ATR-FTIR spectra were collected between 4000 and 900 cm^{-1}. In this wavenumber range, a number of spectral regions assigned to vibrational modes of different functional groups of a lipid molecule can be observed [38–40]. These include the vibration peaks of the polar head groups PO_2^- and $N^+(CH_3)_3$ (the latter only for DPPC), of

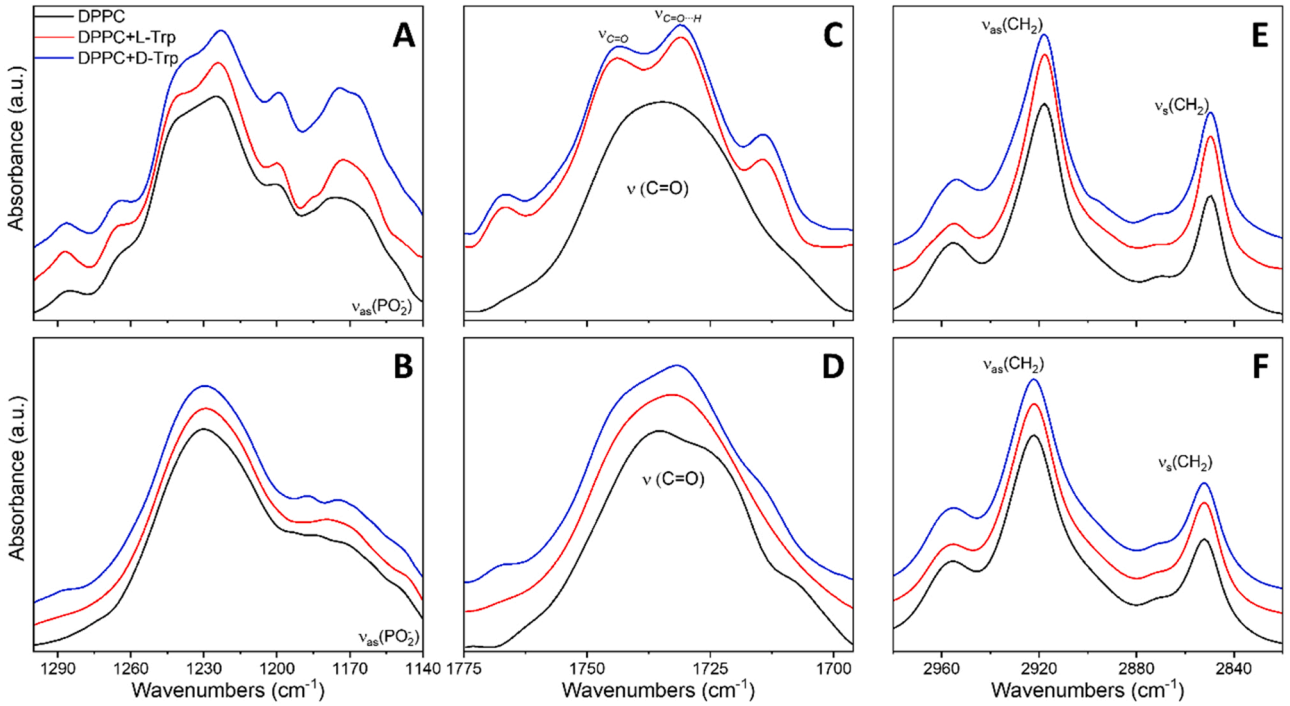

Fig. 3. Representative ATR-FTIR spectra of DPPC bilayers, pure and with Trp enantiomers at 24 °C (A-C-E) and 48 °C (B-D-F) hydrated in DPBS at pH 7.4. PO_2^- asymmetric band (A-B); ester carbonyl C=O stretching band (C-D); methylene CH_2 stretching band (E-F). The spectra are normalized at maximum intensity and vertically shifted to improve visualization. DPPC (bottom line), DPPC+L-Trp (middle line), DPPC+D-Trp (top line). (For interpretation of the references to color in this figure legend, the reader is referred to the web version of this article.)

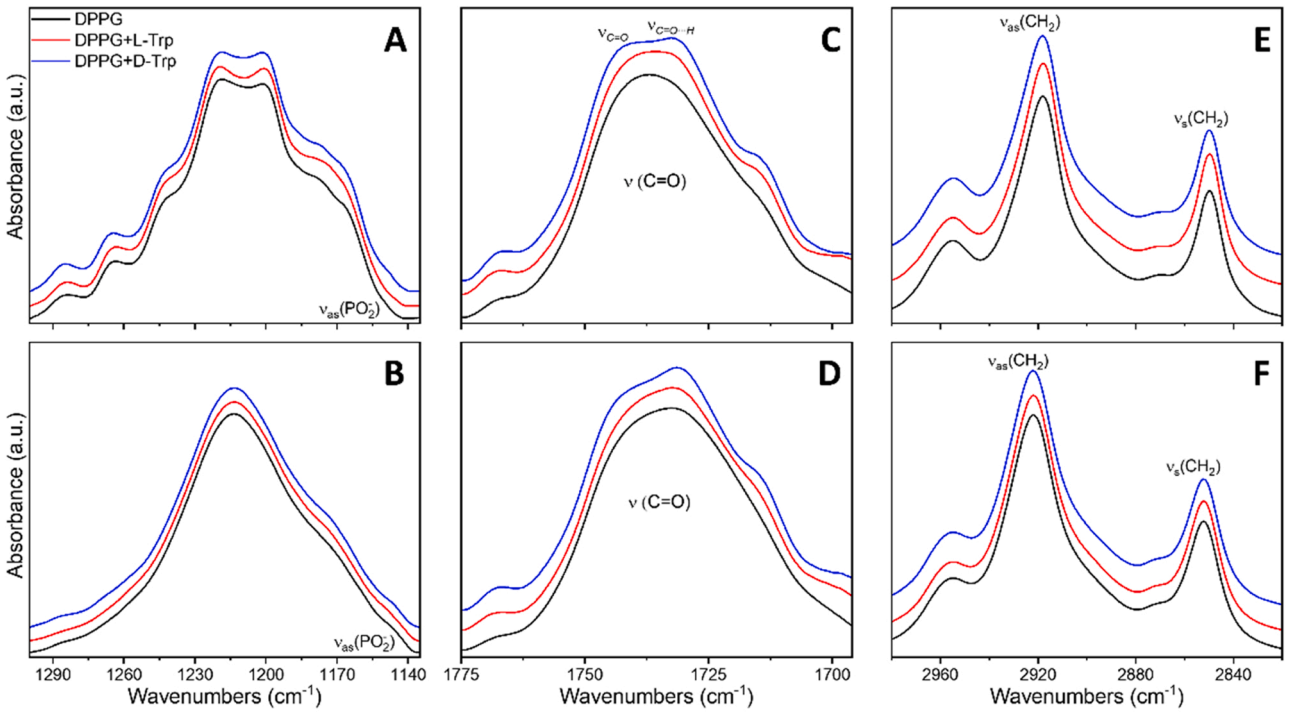

Fig. 4. Representative ATR-FTIR spectra of DPPG bilayers, pure and with Trp enantiomers hydrated in DPBS at pH 7.4 at 24 °C (A-C-E) and 48 °C (B-D-F). PO_2^- asymmetric band (A-B); ester carbonyl C═O stretching band (C-D); methylene CH_2 stretching band (E-F). The spectra are normalized at maximum intensity and vertically shifted to improve visualization. DPPC (bottom line), DPPC+L-Trp (middle line), DPPC+D-Trp (top line). (For interpretation of the references to color in this figure legend, the reader is referred to the web version of this article.)

the interfacial ester C═O groups, and of the hydrocarbon chains CH_2 groups (Figs. 3 and 4). The position of the IR bands of the groups at the polar region and at the polar/apolar interface of the bilayers is sensitive to the formation of hydrogen bonds and/or Coulombic interactions. By following the temperature-induced changes in the wavenumber of hydrocarbon CH_2 bands the lipid phase transitions can be monitored.

Fig. 3A-F show a selection of IR spectral regions of DPPC bilayers without and with Trp enantiomers, at T = 24 °C (i.e., a temperature $T < T_m$ in the gel state) and at T = 48 °C (i.e., a temperature $T > T_m$ in the fluid state).

The lineshape of the absorbance between 1300 and 1140 cm^{-1} of pure DPPC and DPPC in the presence of Trp enantiomers at 24 °C (Fig. 3A) shows several overlapping bands: the PO_2^- asymmetric band at ca. 1225 cm^{-1}, the CH_2 wagging band progressions in the range 1300–1200 cm^{-1}, that are typical of lipids in gel phase with all-trans segments of polymethylene chains, and the CO– O– C asymmetric stretch at 1170 cm^{-1} [38,40,41]. A small downshift of the $\nu_{as}(PO_2^-)$ is recorded with the addition of Trp, particularly for the chiral form D, indicating that the AA promotes formation of hydrogen bonds with the phosphate groups [38]. In accordance with our findings, a downshift of the $(PO_2^-)_{as}$ peak position has been reported for DPPC bilayers interacting with cysteine [42] and for pure bilayers of either PC or PG, as well as for mixed PC/PG bilayers interacting with Trp [43]. For DPPC bilayers at 48 °C, was recorded a large band at ca. 1230 cm^{-1} that is slightly affected by the addition of the Trp stereoisomers (Fig. 3B). This band is essentially due to the PO_2^- asymmetric vibration peak [42,44], since the CH_2 wagging band progressions disappear or are of very low intensity for lipids in the fluid phase with trans-gauge chain isomers [38, 40,41]. A moderate increase up to about 4–5 cm^{-1} of $\nu_{as}(PO_2^-)$ was reported for a variety of model PC membranes on increasing the temperature [40,44,45].

The vibration peak of the $N^+(CH_3)_3$ group of DPPC polar head occurring in the region 900–940 cm^{-1} (spectra not shown) did not display significant differences in the presence of either L-Trp or D-Trp at any temperature.

For DPPC bilayers at $T < T_m$, the broad band in the region between 1775 and 1700 cm^{-1}, corresponding to the lipid carbonyl stretching vibration of the ester C═O group, splits at least into two major components in the presence of the Trp enantiomers (Fig. 3C). The peaks around 1743 and 1730 cm^{-1} were assigned to free, non-hydrogen-bonded ($\nu_{C=O}$) and hydrogen-bonded ($\nu_{C=O\bullet\bullet\bullet H}$) carbonyl groups, respectively [39,46]. For T > Tm, the two components are already evident in the spectrum of pure DPPC, and the addition of Trp in either chiral forms modulates differently their relative intensities (Fig. 3D). The two components of the C═O vibration bands have been resolved by performing a deconvolution of the absorbance on the whole 1775–1770 cm^{-1} range, and quantified by evaluating the area under the component bands. An illustration of the C═O bands deconvolution for DPPC in the absence and in the presence of Trp isomers at 24 °C is given in Fig. S1, and the area ratio of the hydrogen-bonded carbonyls to the free ones, $A(\nu_{C=O\bullet\bullet\bullet H})/A(\nu_{C=O})$, for the samples at 24 °C and 48 °C, is reported in Fig. S2. The area under the curves is proportional to the population of hydrogen-bonded or free C═O groups, and the ratio $A(\nu_{C=O\bullet\bullet\bullet H})/A(\nu_{C=O})$ is used to estimate the fraction of the carbonyls involved in hydrogen-bonding [30,47]. The hydrogen-bonded populations change in the order: DPPC < (DPPC+D-Trp) < (DPPC+L-Trp) and are slightly higher in the liquid-crystalline phase with respect to those in the gel phase (Fig. 3C-D, Figs. S1-S2).

The region between 3000 and 2800 cm^{-1} of the ATR-FTIR spectrum of DPPC at 24 °C (Fig. 3E) is dominated by two peaks around 2850 and 2918 cm^{-1} assigned to symmetric, $\nu_s(CH_2)$, and asymmetric, $\nu_{as}(CH_2)$, methylene stretching vibrations, respectively [40]. These two peaks shift toward higher wavenumbers on increasing temperature, first moderately throughout the gel phase, and then more rapidly on crossing the bilayer main phase transition. For DPPC at 48 °C, the positions of the symmetric and asymmetric bands are around 2852 cm^{-1} and 2922 cm^{-1}, respectively (Fig. 3F). The upshift of the band positions on going from low to high temperatures is indicative of higher conformational disorder

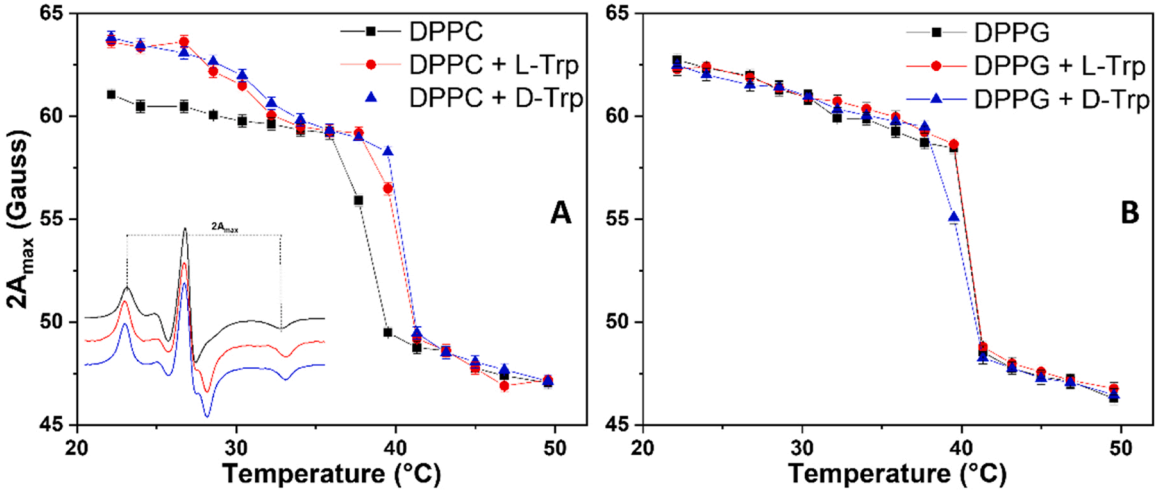

Fig. 5. (A) Temperature dependences of the outer hyperfine separation, $2A_{max}$, for 4-PCSL in bilayers of DPPC without (squares) and with either L-Trp (circles) or D-Trp (triangles) hydrated in DPBS at pH 7.4. Inset: ESR spectra of 4-PCSL at 22 °C in DPPC; from top to bottom: lipid alone (black line), lipid with L-Trp (red line), lipid with D-Trp (blue line). (B) As in (A) but for DPPG. (For interpretation of the references to color in this figure legend, the reader is referred to the web version of this article.)

and mobility of the DPPC hydrocarbon chains, for the presence of trans/gauche conformers in the fluid phase. At the same time, an increase in bandwidth of the CH_2 antisymmetric asymmetric stretching modes is also observed with temperature increase, related to enhanced motional rates and a larger number of conformational states of the acyl chains in the fluid phase (see Fig. 3E-F). Similar upshifts of $\nu_s(CH_2)$ and variations of the bandwidths are usually reported at the main phase transitions in model membranes of various lipid composition and hydration level (either dry and rehydrated) [40,47,48]. Moreover, $\nu_s(CH_2)$ upshift with temperature increase are reported in lipid bilayers interacting with AAs [42,43,49,50] and other ligands [51,52]. The two peak positions, both in the gel and in the liquid state of DPPC, do not significantly change with the addition of L- and D-Trp (Fig. 3E-F).

Apart from the vibration $N^+(CH_3)_3$ peak, the vibrational modes of the same functional groups were analyzed in the case of the negatively charged DPPG membrane without and with L-/D-Trp (Fig. 4A-F).

The contours of the absorbance for DPPG ± L-/D-Trp in the 1300–1140 cm^{-1} region (Fig. 4 A-B) are characterized by the presence of several bands, as occurred in the case of DPPC. The PO_2^- asymmetric stretching peak is at ca. 1201 cm^{-1} for membranes in the gel phase at 24 °C, and is upshifted at ca. 1214 cm^{-1} in the fluid phase at 48 °C (Fig. 4B), in close accordance with literature data [39,53]. The bands do not show appreciable differences upon the addition of Trp enantiomers, at both $T < T_m$ and $T > T_m$ (Fig. 4A-B). It is interesting to note that PG bilayers undergo larger $\nu(PO2)_{as}$ upshift on increasing the temperature with respect to PC bilayers, because the phosphate group is involved in hydrogen-bonding with the glycerol hydroxyls of the polar head [39].

As in the case of DPPC, the ester C═O stretching bands of DPPG at low ($T < T_m$) and high ($T > T_m$) temperature are rather large and are mainly due to the superposition of unresolved free and hydrogen-bonded carbonyl group components (Fig. 4C-D). The two populations showed up in the presence of Trp enantiomers, with the hydrogen-bonded one more clearly visible at 48 °C in any sample. These observations are also confirmed by the quantitative analysis of the curve deconvolutions (see Figs. S1-S2). Indeed, it indicates that in DPPG bilayers the fractions of hydrogen-bonded populations change in the order: DPPG < (DPPG+L-Trp) ≈ (DPPG+D-Trp) (i.e., they increase to the same extent in the presence of L- and D-Trp), and are higher in the liquid-crystalline phase.

As the neutral DPPC and the anionic DPPG membrane have saturated chains of the same length, the $\nu_s(CH_2)$ and $\nu_{as}(CH_2)$ stretching vibration bands of DPPG chains (Fig. 4E-F) are located at the same wavenumbers as for DPPC and the temperature increase led to a similar increase of the band positions towards higher wavenumbers [45,52]. The Trp enantiomers did not induce any significant change in the CH_2 stretching band in terms of position and shape (see Fig. 4E-F).

The ATR-FTIR give indication that the Trp enantiomers interact preferentially and differently with the head groups and the polar-apolar interface of DPPC and DPPG bilayers mainly for temperature through the gel state, whereas they leave unperturbed the hydrocarbon region of the bilayers at any temperature.

3.3. Spin-label electron spin resonance spectroscopy

To get insight into the effects of Trp enantiomers at different depth in the hydrophobic interior of the membrane, we performed temperature-dependent ESR measurements of chain-labeled lipids inserted into the membrane to probe the first acyl chain segments (by using 4-PCSL) and the inner hydrocarbon region at the bilayer center (by using 14-PCSL).

In any sample (DPPC or DPPG, without or with Trp), the spectra of 4-PCSL (Fig. S3) displayed a temperature-dependent decrease of the spectral anisotropy, which is more accentuated on crossing the phase transitions, particularly the main one. This is due to the temperature-induced increased rotational mobility and loosened packing density of the segmental lipid chains. The ESR spectra were quantitatively analyzed by evaluating the outer hyperfine separation, $2A_{max}$, corresponding to the separation between the low-field maximum and the high-field minimum resonances (see inset to Fig. 5A). This parameter reflects the amplitude and the rate of motion in all motional regimes of the conventional ESR timescale [54]. The larger the anisotropy, the greater the $2A_{max}$ value and the higher the order due to the motional restriction of the lipid chain.

For 4-PCSL in zwitterionic DPPC bilayers a similar increase of the spectral anisotropy or $2A_{max}$ is observed in the presence of both L- and D-Trp for temperatures through the gel phase. This is evident in the ESR spectra reported in Fig. S3, in the spectra at 22 °C reported in the inset to Fig. 5 A, and in the plots of $2A_{max}$ versus temperature in Fig. 5 A. The ESR data indicate that both forms of the Trp enantiomers, upon interacting with DPPC bilayers, promote a denser packing density and motional restriction of the segmental lipid chains in the gel state, without perturbing the zwitterionic DPPC bilayers in the liquid-crystalline state. Furthermore, from the comparison of the plots in Fig. 5 A, it is evident that both AA enantiomers make more evident the pre-transition and upshift the main phase transition temperature, thus

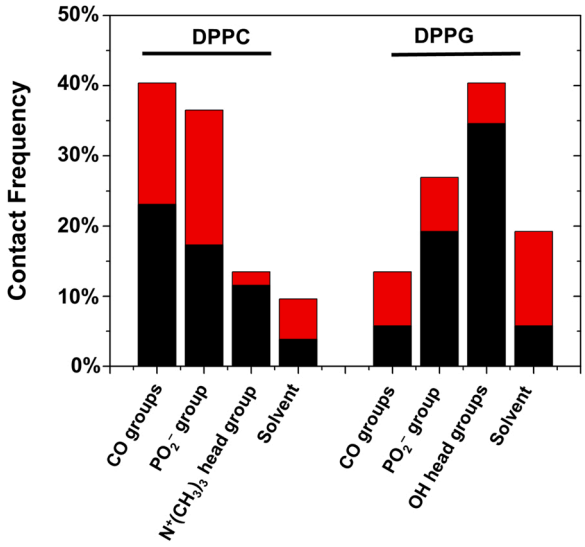

Fig. 6. Frequency of the contacts of the polar H atoms of both Trp enantiomers with the two phospholipids DPPC and DPPG, as observed in molecular docking. Contacts of both the NH_3^+ amino group (black) and the NH (red) in the side chain of Trp are reported, in interaction with two phospholipid molecules of either DPPC (left) or DPPG (right). Contacts are divided into hydrogen bonds with the CO groups, with the PO_2^- group, electrostatic interactions with the head group region ($N^+(CH3)_3$ moiety in DPPC, and two OH groups in DPPG; see also Fig. 1), and contacts with the solvent (i.e., solvent-exposed polar H atoms of Trp). (For interpretation of the references to color in this figure legend, the reader is referred to the web version of this article.)

stabilizing the membrane gel state.

For 4-PCSL in anionic DPPG bilayers, both L- and D-Trp induce slight modifications in the temperature dependence of the spectral anisotropy and in the value of $2A_{max}$ in the gel phase, and leave them almost unaffected in the fluid phase (Figs. S3 and 5B).

The spectra of 14-PCSL in both DPPC and DPPG bilayers at any temperature (Fig. S4) display a lower anisotropy compared to the corresponding spectra of 4-PCSL in the same lipid matrices. This is expected when the nitroxide moiety probes the inner hydrocarbon regions characterized by enhanced segmental lipid chain disorder and mobility, relative to the first acyl chain segments probed by 4-PCSL. For DPPC/14-PCSL and DPPG/14-PCSL, the extent of spectral anisotropy decreases continuously on increasing the temperature from the gel to the liquid crystalline phase where the spectra, because of the high degree of motional narrowing, resemble almost isotropic triplets with differential line broadening, as it normally occurs for an end-chain spin-labeled lipid such as 14-PCSL. The spectra of 14-PCSLin the neutral and negatively charged membranes are slightly affected by the addition of L- and D-Trp.

The spin-label ESR findings clearly indicate that the Trp enantiomers affect differently and in an aspecific way the lipid bilayers as a function of temperature: both L- and D-Trp increase the order of the upper chain segments of DPPC in the gel state but not of DPPG; moreover, they do not penetrate the inner hydrophobic zone of DPPC and DPPG bilayers at any temperature.

3.4. Molecular docking simulation

Molecular docking was used to obtain indications at atomic detail that complement our spectroscopic data and contribute to characterize the interaction of the Trp enantiomers with DPPC and DPPG membranes.

The *in silico* experiments showed that Trp has a tendency to bind two phospholipid molecules at the same time, both in the interaction with DPPC and DPPG. In fact, the AA tends to be sandwiched between two phospholipid molecules, whereas the simultaneous docking of a third phospholipid resulted in the binding of such additional molecule to either of the other two phospholipids already present (or both, in some rare cases), with little or no interaction with the Trp. This finding is in agreement with a previous study that explored the binding of Trp to DPPC, where a 1:2 stoichiometry of interaction was hypothesized on the basis of a lock-and-key model conceived solely on geometrical considerations on the possible formation of hydrogen bonds [3].

In our computations, the binding affinity of Trp for DPPC was slightly less favorable than for DPPG (up to −3.0 and −3.5 kcal/mol, respectively). These values are in line with indications obtained by using molecular dynamics simulations to estimate the energetic of transfer of AAs from water to lipid interfaces [33], which yielded slightly more favorable interfacial partitioning (−5.2 kcal/mol for DOPC). The binding energy values obtained in simulation are rather weak, but sufficient to encourage the binding of Trp to the membranes, or at least the dynamical transfer of a fraction of it from the aqueous medium. As regards a possible difference between the two Trp enantiomers in the binding, we did not observe any appreciable distinction, except a very small tendency of L-Trp to bind with a more favorable affinity (0.1–0.2 kcal/mol) and slightly closer to the lipid/water interface compared to D-Trp. Therefore, we combined the results obtained for both enantiomers, to increase the statistical significance of our data in the subsequent analysis.

Fig. 6 shows the distribution of the atomic contacts observed between polar hydrogens of both Trp enantiomers (i.e., the contacts involving both the NH_3^+ amino group and the NH moiety in the side chain of Trp, see Fig. 1A) and either DPPC or DPPG. In terms of molecular interactions, these contacts consist of hydrogen bonds formed with the CO group and with the PO_2^- group (that are equally present in the two phospholipid species), and electrostatic interactions with the polar head region of either DPPC or DPPG, which include the possibility of forming hydrogen bonds with the two OH groups of DPPG (Fig. 1), or favorable Coulombic interactions with the charged $N^+(CH_3)_3$ moiety of the choline at the surface extremity of DPPC. Furthermore, it was assumed that solvent-exposed hydrogen bond donors of Trp not found in any contact with the phospholipids would tend to coordinate water molecules and, therefore, were counted as contacts with the solvent. The hydrogen bonds formed in all cases were very weak, as it could be deduced by the little favorable binding energy of Trp towards both DPPC and DPPG (see discussion above), and by their suboptimal geometry found in the docking (data not shown).

Our data on the atomic contacts formed by Trp, reported in Fig. 6, show that the AA inserts deeper in the DPPC membrane compared to DPPG. For both phospholipid species there is an appreciable amount of weak hydrogen bonds formed with the CO groups and with the PO_2^- group, in agreement with our experimental ATR-FTIR data. The largest difference was observed in the contacts with the upper surface region of the two phospholipids, and it is driven by the larger conformational flexibility and the possibility of accepting hydrogen bonds for the OH moieties of the glycerol head group of DPPG, at variance with DPPC that does not possess such moieties in the head group.

The contacts of Trp with solvent are also more frequent when the AA is bound to DPPG compared to DPPC. It is also clear from the data that Trp forms a larger number of contacts with its NH_3^+ amino group rather than with its side chain NH group, as a consequence of the higher number of H atoms in the former that are able to be simultaneously involved in hydrogen bond interactions with the phospholipid molecules.

4. Discussion and conclusions

This work helps to shed light on the molecular mechanisms that regulate the interaction between model membranes and Trp enantiomers. On the whole, our experimental and computational results indicate that L- and D-Trp interact with neutral DPPC and anionic DPPG bilayers and affects their molecular properties, such as the thermotropic

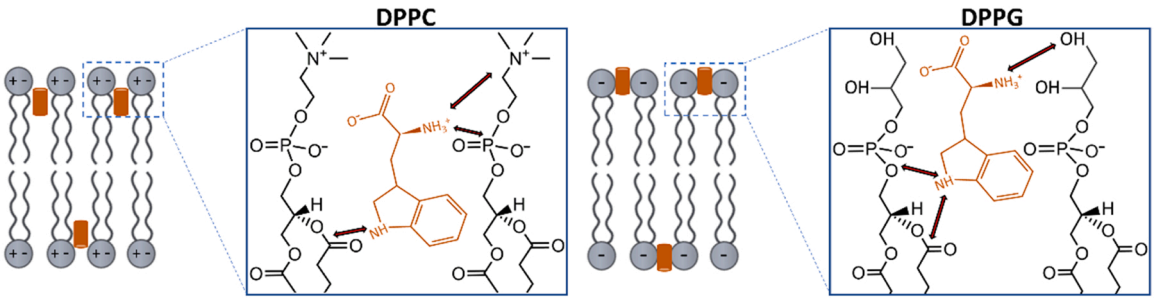

Fig. 7. Schematic representation of the interactions of Trp with DPPC (left) and DPPG (right). The different vertical location of Trp in the two lipid matrices is also shown.

phase behavior, hydrogen bond formation, and chain packing density. Both Trp enantiomers slightly affect the bilayer phase transition characteristics, producing variations mainly in the enthalpy values. Their presence also induces alterations of the IR spectra related to molecular groups located at the lipid surfaces and at the polar/apolar region, promoting hydrogen bonds formation and possibly (weak) electrostatic interactions. Furthermore, for temperatures in the gel state, the Trp chiral forms perturb the order and mobility of the upper hydrocarbon region of DPPC but not that of DPPG bilayers. In contrast, in any sample, they do not perturb the inner hydrocarbon region of both bilayers at any temperature.

The most likely explanation of the overall results is that L- and D-Trp associate at the polar head and at the interfacial regions of the membranes, without penetrating deeply in the hydrocarbon core of the lipid bilayers. This is a behavior also occurring for other small ligands and drugs previously investigated by us, such as resveratrol, ibuprofen and warfarin [55–57] as well as by other authors, such as flavonol glycosides [30] or statine and various prodrugs [45,52]. All these ligands bind on the surface of a variety of lipid membranes and induce slight variations in the membrane properties without compromising their integrity. In the case of Trp, our results are in close agreement with a number of studies that claim this AA localizes in the interfacial region of lipid bilayers [21, 23,33]. It has been reported that the preference of Trp to locate in the complex interfacial environment of dry and rehydrated membranes affects the hydrogen-bonds network and the interactions at the lipid head groups [43,49]. Further, both experiment and simulations suggested that tryptophan resides near the glycerol linkage of the DOPC lipid, where it is likely stabilized by multiple electrostatic and hydrogen-bonding interactions in the near-surface region of the membrane [23]. It is also worthy of note that Trp in membrane proteins is located preferentially at the lipid membrane interface [58,59], thus favoring protein insertion and anchoring. The location of Trp in lipid membranes proposed on the basis of our data may be due to a balance among hydrophobic effects that repel it from the surrounding water, electrostatic interactions that favor its insertion in the hydrated head group region, and cohesive repulsion of the lipid hydrocarbon chains that keeps the AA out of the hydrocarbon core.

As surface-adsorbing molecules, the influence of Trp on the membrane is more evident for temperatures in which the lipids are in the gel state, where the area per polar head is lower, and negligible in the liquid-crystalline state. The different type of the lipid polar heads, i.e., PC versus PG, plays a role in modulating the location of Trp in the lipid membranes. In fact, Trp in DPPG bilayers maintains a more superficial association favored by contacts with the OH glycerol groups of the polar head, whereas in DPPC it penetrates deeper and it mainly interacts with the interfacial region, promoting denser packing of the first acyl chain segments. This is also the main distinction found in simulation for the binding of Trp to each membrane: a higher propensity for hydrogen bond with the phosphate group in DPPC and a preference in the formation of interactions with the glycerol group in DPPG. The different sites of association and interactions, established by Trp in the two membranes, are also reflected in the slight enthalpy changes reported by our DSC measurements. Indeed, the higher ΔH values relative to pure DPPC indicate a Trp-induced stabilization of the lipid matrix. Such a stabilization is also evidenced in the increased order of the upper hydrocarbon chains detected with spin-label ESR (Fig. 5 A). The lower ΔH values relative to pure DPPG suggest that the AA, by interacting mainly with the membrane surface regions, likely promotes a looser intermolecular packing of the polar heads. In Fig. 7 is shown a scheme of the favored interactions of Trp with the zwitterionic DPPC and anionic DPPG bilayers, illustrating also the different vertical location of the AA in the membranes.

It is also interesting to observe that our simulation clearly indicates that the binding of this AA takes place in a region that includes the chiral center of the two phospholipid species. Therefore, this observation indirectly suggests the potential source of enantioselectivity in the binding observed for DPPC membranes with L-Trp versus D-Trp [3], although the molecular details of such preferences are still not clear.

In conclusion, our results contribute to a better understanding of the interaction between chiral biomolecules and the occurrence of stereospecific effects. Further study will be devoted to investigate the role of membrane composition complexity in chiral recognition of active biomolecules, such as AAs. Such studies can also pave the way for biomedical and pharmaceutical applications where the separation, asymmetric recognition, and detection of chiral biomarkers and drugs are desirable.

CRediT authorship contribution statement

All authors designed research; **A.G., R.B., R.G.** performed experiments; **B.R.** performed docking; **A.G., R.B.. R.G., B.R.** analyzed data; **A. G.** wrote the first draft; **R.B** and B.R. wrote the manuscript (review & editing); all authors read and approved the manuscript.

Declaration of Competing Interest

The authors declare that they have no known competing financial interests or personal relationships that could have appeared to influence the work reported in this paper.

Data availability

Data will be made available on request.

Acknowledgements

A.G. acknowledges financial support from the “NLHT- Nanoscience Laboratory for Human Technologies” - (POR Calabria FESR-FSE 14/20).

Appendix A. Supporting information

Supplementary data associated with this article can be found in the

online version at doi:10.1016/j.colsurfb.2023.113216.

References

[1] U. Kragh-Hansen, V.T.G. Chuang, M. Otagiri, Practical aspects of the ligand-binding and enzymatic properties of human serum albumin, Biol. Pharm. Bull. 25 (2002) 695–704, https://doi.org/10.1248/bpb.25.695.

[2] H. Tsuchiya, Stereospecificity in membrane effects of catechins, Chem. Biol. Interact. 134 (2001) 41–54, https://doi.org/10.1016/S0009-2797(00)00308-2.

[3] T. Ishigami, K. Suga, H. Umakoshi, Chiral recognition of L-amino acids on liposomes prepared with L-phospholipid, ACS Appl. Mater. Interfaces 7 (2015) 21065–21072, https://doi.org/10.1021/acsami.5b07198.

[4] Y. Okamoto, Y. Kishi, T. Ishigami, K. Suga, H. Umakoshi, Chiral selective adsorption of ibuprofen on a liposome membrane, J. Phys. Chem. B 120 (2016) 2790–2795, https://doi.org/10.1021/acs.jpcb.6b00840.

[5] T. Ishigami, A. Tauchi, K. Suga, H. Umakoshi, Effect of boundary edge in DOPC/DPPC/cholesterol liposomes on acceleration of l-histidine preferential adsorption, Langmuir 32 (2016) 6011–6019, https://doi.org/10.1021/acs.langmuir.5b04626.

[6] P. Gusain, S. Ohki, K. Hoshino, Y. Tsujino, N. Shimokawa, M. Takagi, Chirality-dependent interaction of D-and L-menthol with biomembrane models, Membranes 7 (2017) 69, https://doi.org/10.3390/membranes7040069.

[7] A.V. Mastova, O.Y. Selyutina, N.E. Polyakov, Stereoselectivity of Interaction of Nonsteroidal Anti-Inflammatory Drug S-Ketoprofen with L/D-Tryptophan in Phospholipid Membranes, Membranes 12 (2022) 460, https://doi.org/10.3390/membranes12050460.

[8] H. Takase, K. Suga, H. Matsune, H. Umakoshi, K. Shiomori, Preferential adsorption of L-tryptophan by L-phospholipid coated porous polymer particles, Colloids Surf. B Biointerfaces 216 (2022), 112535, https://doi.org/10.1016/j.colsurfb.2022.112535.

[9] H. Tsuchiya, M. Mizogami, The membrane interaction of drugs as one of mechanisms for their enantioselective effects, Med. Hypotheses 79 (2012) 65–67, https://doi.org/10.1016/j.mehy.2012.04.001.

[10] T. Eriksson, S. Björkman, P. Höglund, Clinical pharmacology of thalidomide, Eur. J. Clin. Pharmacol. 57 (2001) 365–376, https://doi.org/10.1007/s002280100320.

[11] J. Guo, X. Wei, H. Lian, L. Li, X. Sun, B. Liu, Urchin-like chiral metal–organic framework/reduced graphene oxide nanocomposite for enantioselective discrimination of d/l-tryptophan, ACS Appl. Nano Mater. 3 (2020) 3675–3683, https://doi.org/10.1021/acsanm.0c00389.

[12] R. Huang, K. Shen, Q. He, Y. Hu, C. Sun, C. Guo, Y. Pan, Metabolic profiling of urinary chiral amino-containing biomarkers for gastric cancer using a sensitive chiral chlorine-labeled probe by HPLC-MS/MS, J. Proteome Res. 20 (2021) 3952–3962, https://doi.org/10.1021/acs.jproteome.1c00267.

[13] A. Lininger, G. Palermo, A. Guglielmelli, G. Nicoletta, M. Goel, M. Hinczewski, G. Strangi, Chirality in light-matter interaction, Adv. Mater. 2107325 (2022), https://doi.org/10.1002/adma.202107325.

[14] T. Kimura, K. Hamase, Y. Miyoshi, R. Yamamoto, K. Yasuda, M. Mita, H. Rakugi, T. Hayashi, Y. Isaka, Chiral amino acid metabolomics for novel biomarker screening in the prognosis of chronic kidney disease, Sci. Rep. 6 (2016) 1–7, https://doi.org/10.1038/srep26137.

[15] Y. Liu, Z. Wu, P.S. Kollipara, R. Montellano, K. Sharma, Y. Zheng, Label-free ultrasensitive detection of abnormal chiral metabolites in diabetes, ACS Nano 15 (2021) 6448–6456, https://doi.org/10.1021/acsnano.0c08822.

[16] G. Palermo, G. Strangi, Biomolecular Sensing in Hybrid Chiral/Hyperbolic Metastructures, Hybrid Flatland Metastructures, AIP Publishing, Melville, New York, 2021, 11-11-11-14.

[17] G.D. Ciccotosto, D.J. Tew, S.C. Drew, D.G. Smith, T. Johanssen, V. Lal, T.-L. Lau, K. Perez, C.C. Curtain, J.D. Wade, Stereospecific interactions are necessary for Alzheimer disease amyloid-β toxicity, Neurobiol. Aging 32 (2011) 235–248, https://doi.org/10.1016/j.neurobiolaging.2009.02.018.

[18] M. Friedman, Analysis, nutrition, and health benefits of tryptophan (1178646918802282). Int. J. Tryptophan Res. 11 (2018) https://doi.org/10.1177/1178646918802282.

[19] N. Erbilen, E. Zor, A.O. Saf, E.G. Akgemci, H. Bingol, An electrochemical chiral sensor based on electrochemically modified electrode for the enantioselective discrimination of D-/L-tryptophan, J. Solid State Electrochem. 23 (2019) 2695–2705, https://doi.org/10.1007/s10008-019-04370-x.

[20] S. Barik, The uniqueness of tryptophan in biology: properties, metabolism, interactions and localization in proteins, Int. J. Mol. Sci. 21 (2020) 8776, https://doi.org/10.3390/ijms21228776.

[21] S. Persson, J.A. Killian, G. Lindblom, Molecular ordering of interfacially localized tryptophan analogs in ester-and ether-lipid bilayers studied by ^{2}H NMR, Biophys. J. 75 (1998) 1365–1371, https://doi.org/10.1016/S0006-3495(98)74054-8.

[22] A.V. Popova, A.G. Heyer, D.K. Hincha, Differential destabilization of membranes by tryptophan and phenylalanine during freezing: the roles of lipid composition and membrane fusion, Biochim. Biophys. Acta Biomembr. 1561 (2002) 109–118, https://doi.org/10.1016/S0005-2736(01)00462-X.

[23] C.M. Anderson, A. Cardenas, R. Elber, L.J. Webb, Preferential equilibrium partitioning of positively charged tryptophan into phosphatidylcholine bilayer membranes, J. Phys. Chem. B 123 (2019) 170–179, https://doi.org/10.1021/acs.jpcb.8b09872.

[24] M. Robinson, S. Turnbull, B.Y. Lee, Z. Leonenko, The effects of melatonin, serotonin, tryptophan and NAS on the biophysical properties of DPPC monolayers, Biochim. Biophys. Acta Biomembr. 1862 (2020), 183363, https://doi.org/10.1016/j.bbamem.2020.183363.

[25] J. Martí, H. Lu, Microscopic interactions of melatonin, serotonin and tryptophan with zwitterionic phospholipid membranes, Int. J. Mol. Sci. 22 (2021) 2842, https://doi.org/10.3390/ijms22062842.

[26] G. Van Meer, D.R. Voelker, G.W. Feigenson, Membrane lipids: where they are and how they behave, Nat. Rev. Mol. Cell Biol. 9 (2008) 112–124, https://doi.org/10.1038/nrm2330.

[27] D. Marsh, A. Watts, Spin-labeling and lipid-protein interactions in membranes. Lipid-protein Interactions, Wiley- Interscience, New York, 1982, pp. 53–126.

[28] D.D. Lasic, Liposomes: from Physics to Applications, Elsevier Science Limited, Amsterdam, 1993.

[29] S.C. Gill, P.H.Von Hippel, Calculation of protein extinction coefficients from amino acid sequence data, Anal. Biochem. 182 (1989) 319–326, https://doi.org/10.1016/0003-2697(89)90602-7.

[30] A.V. Popova, D.K. Hincha, Effects of flavonol glycosides on liposome stability during freezing and drying, Biochim. Biophys. Acta - Biomembr. 1858 (2016) 3050–3060, https://doi.org/10.1016/j.bbamem.2016.09.020.

[31] J. Eberhardt, D. Santos-Martins, A.F. Tillack, S. Forli, AutoDock Vina 1.2. 0: new docking methods, expanded force field, and python bindings, J. Chem. Inf. Model. 61 (2021) 3891–3898, https://doi.org/10.1021/acs.jcim.1c00203.

[32] S. Kim, J. Chen, T. Cheng, A. Gindulyte, J. He, S. He, Q. Li, B.A. Shoemaker, P. A. Thiessen, B. Yu, PubChem in 2021: new data content and improved web interfaces, Nucleic Acids Res. 49 (2021) D1388–D1395, https://doi.org/10.1093/nar/gkaa971.

[33] J.L. MacCallum, W.D. Bennett, D.P. Tieleman, Partitioning of amino acid side chains into lipid bilayers: results from computer simulations and comparison to experiment, J. Gen. Physiol. 129 (2007) 371–377, https://doi.org/10.1085/jgp.200709745.

[34] F. Grande, B. Rizzuti, M.A. Occhiuzzi, G. Ioele, T. Casacchia, F. Gelmini, R. Guzzi, A. Garofalo, G. Statti, Identification by molecular docking of homoisoflavones from Leopoldia comosa as ligands of estrogen receptors, Molecules 23 (2018) 894, https://doi.org/10.3390/molecules23040894.

[35] O. Trott, A.J. Olson, AutoDock Vina: improving the speed and accuracy of docking with a new scoring function, efficient optimization, and multithreading, J. Comput. Chem. 31 (2010) 455–461, https://doi.org/10.1002/jcc.21334.

[36] M.H. Chiu, E.J. Prenner, Differential scanning calorimetry: an invaluable tool for a detailed thermodynamic characterization of macromolecules and their interactions, J. Pharm. BioAllied Sci. 3 (2011) 39, https://doi.org/10.4103/0975-7406.76463.

[37] D. Marsh. Handbook of Lipid Bilayers, second ed., CRC Press, Boca Raton, 2013.

[38] J.L.R. Arrondo, F.M. Goñi, J.M. Macarulla, Infrared spectroscopy of phosphatidylcholines in aqueous suspension a study of the phosphate group vibrations, Biochim. Biophys. Acta 794 (1984) 165–168, https://doi.org/10.1016/0005-2760(84)90310-2.

[39] R.N.A.H. Lewis, R.N. McElhaney, The structure and organization of phospholipid bilayers as revealed by infrared spectroscopy, Chem. Phys. Lipids 96 (1998) 9–21, https://doi.org/10.1016/S0009-3084(98)00077-2.

[40] R.N.A.H. Lewis, R.N. McElhaney, Membrane lipid phase transitions and phase organization studied by Fourier transform infrared spectroscopy, Biochim. Biophys. Acta - Biomembr. 1828 (2013) 2347–2358, https://doi.org/10.1016/j.bbamem.2012.10.018.

[41] L.K. Tamm, S.A. Tatulian, Infrared spectroscopy of proteins and peptides in lipid bilayers, Q. Rev. Biophys. 30 (1997) 365–429, https://doi.org/10.1017/S0033583597003375.

[42] J.M. Arias, M.E. Tuttolomondo, S.B. Díaz, A. Ben Altabef, Reorganization of hydration water of DPPC multilamellar vesicles induced by l-cysteine interaction, J. Phys. Chem. B 122 (2018) 5193–5204, https://doi.org/10.1021/acs.jpcb.8b01721.

[43] A.V. Popova, D.K. Hincha, Specific interactions of tryptophan with phosphatidylcholine and digalactosyldiacylglycerol in pure and mixed bilayers in the dry and hydrated state, Chem. Phys. Lipids 132 (2004) 171–184, https://doi.org/10.1016/j.chemphyslip.2004.06.003.

[44] A.V. Popova, D.K. Hincha, Intermolecular interactions in dry and rehydrated pure and mixed bilayers of phosphatidylcholine and digalactosyldiacylglycerol: a Fourier transform infrared spectroscopy study, Biophys. J. 85 (2003) 1682–1690, https://doi.org/10.1016/S0006-3495(03)74598-6.

[45] E. Sariisik, M. Koçak, F.K. Baloglu, F. Severcan, Interaction of the cholesterol reducing agent simvastatin with zwitterionic DPPC and charged DPPG phospholipid membranes, Biochim. Biophys. Acta - Biomembr. 1861 (2019) 810–818, https://doi.org/10.1016/j.bbamem.2019.01.014.

[46] A. Blume, W. Hübner, G. Messner, Fourier transform infrared spectroscopy of 13C: O labeled phospholipids hydrogen bonding to carbonyl groups, Biochemistry 27 (1988) 8239–8249, https://doi.org/10.1021/bi00421a038.

[47] A.V. Popova, D.K. Hincha, Effects of cholesterol on dry bilayers: interactions between phosphatidylcholine unsaturation and glycolipid or free sugar, Biophys. J. 93 (2007) 1204–1214, https://doi.org/10.1529/biophysj.107.108886.

[48] A.V. Popova, D.K. Hincha, Effects of the sugar headgroup of a glycoglycerolipid on the phase behavior of phospholipid model membranes in the dry state, Glycobiology 15 (2005) 1150–1155, https://doi.org/10.1093/glycob/cwj001.

[49] A.V. Popova, D.K. Hincha, Interactions of the amphiphiles arbutin and tryptophan with phosphatidylcholine and phosphatidylethanolamine bilayers in the dry state, BMC Biophys. 6 (2013) 1–10, https://doi.org/10.1186/2046-1682-6-9.

[50] J.M. Arias, M.E. Tuttolomondo, S.B. Díaz, A.B. Altabef, FTIR and Raman analysis of l-cysteine ethyl ester HCl interaction with dipalmitoylphosphatidylcholine in anhydrous and hydrated states, J. Raman Spectrosc. 46 (2015) 369–376, https://doi.org/10.1002/jrs.4659.

[51] E. Mateos-Diaz, J.-C.B. N'goma, D. Byrne, S. Robert, F. Carrière, H. Gaussier, IR spectroscopy analysis of pancreatic lipase-related protein 2 interaction with phospholipids: 1. Discriminative recognition of mixed micelles versus liposomes, Chem. Phys. Lipids 211 (2018) 52–65, https://doi.org/10.1016/j.chemphyslip.2017.02.005.

[52] G.C. Arslan, F. Severcan, The effects of radioprotectant and potential antioxidant agent amifostine on the structure and dynamics of DPPC and DPPG liposomes, Biochim. Biophys. Acta Biomembr. 1861 (2019) 1240–1251, https://doi.org/10.1016/j.bbamem.2019.04.009.

[53] Y.-P. Zhang, R.N.A.H. Lewis, R.N. McElhaney, Calorimetric and spectroscopic studies of the thermotropic phase behavior of the n-saturated 1, 2-diacylphosphatidylglycerols, Biophys. J. 72 (1997) 779–793, https://doi.org/10.1016/S0006-3495(97)78712-5.

[54] D. Marsh. Spin-label Electron Paramagnetic Resonance Spectroscopy, first ed., CRC Press, Boca Raton, 2019.

[55] E. Longo, F. Ciuchi, R. Guzzi, B. Rizzuti, R. Bartucci, Resveratrol induces chain interdigitation in DPPC cell membrane model systems, Colloids Surf. B. Biointerfaces 148 (2016) 615–621, https://doi.org/10.1016/j.colsurfb.2016.09.040.

[56] E. Aloi, B. Rizzuti, R. Guzzi, R. Bartucci, Association of ibuprofen at the polar/apolar interface of lipid membranes, Arch. Biochem. Biophys. 654 (2018) 77–84, https://doi.org/10.1016/j.abb.2018.07.013.

[57] E. Aloi, B. Rizzuti, R. Guzzi, R. Bartucci, Binding of warfarin differently affects the thermal behavior and chain packing of anionic, zwitterionic and cationic lipid membranes, Arch. Biochem. Biophys. 694 (2020), 108599, https://doi.org/10.1016/j.abb.2020.108599.

[58] H. Sun, D.V. Greathouse, O.S. Andersen, R.E. Koeppe, The preference of tryptophan for membrane interfaces: insights from N-methylation of tryptophans in gramicidin channels, J. Biol. Chem. 283 (2008) 22233–22243, https://doi.org/10.1074/jbc.M802074200.

[59] W.-M. Yau, W.C. Wimley, K. Gawrisch, S.H. White, The preference of tryptophan for membrane interfaces, Biochemistry 37 (1998) 14713–14718, https://doi.org/10.1021/bi980809c.